CHEMISTRY
A EUROPEAN JOURNAL

DOI: 10.1002/chem.201002069

Pentanary Cross-Diffusion in Water-in-Oil Microemulsions Loaded with Two Components of the Belousov–Zhabotinsky Reaction

Federico Rossi,[a, b] Vladimir K. Vanag,[a, c] and Irving R. Epstein*[a]

Abstract: We measure cross-diffusion coefficients in a five-component system, an aerosol OT (AOT) water-in-oil microemulsion loaded with two constituents of the Belousov–Zhabotinsky (BZ) reaction (H_2O/AOT/BZ1/BZ2/octane). The species BZ1 is either NaBr, an inhibitor of the BZ reaction, or ferroin, a catalyst for the reaction. As species BZ2, we choose Br_2, an intermediate in the reaction. The cross-diffusion coefficients between BZ1 and BZ2 are found to be negative, which can be understood in terms of complexation between these species. Using a four-variable model for the BZ reaction, we find that the cross-diffusion coefficients measured here can lead to a noticeable shift in the onset of Turing instability in the BZ–AOT system.

Keywords: Belousov–Zhabotinsky reaction · diffusion · dissipative processes · reverse microemulsions · Taylor dispersion

Introduction

Cross-diffusion, the phenomenon in which a flux of one species is induced by a concentration gradient of another species, can affect or even induce dissipative patterns in reaction-diffusion systems.[1] There are at least two major categories of mechanisms that can lead to cross-diffusion: complexation, for example, between an enzyme and a substrate, or between a "host" and a "guest", or due to electrostatic interaction between ions; and excluded volume, due to the fact that one species at relatively large concentrations can restrict the free space for diffusion of another, thereby increasing the latter's effective local concentration. In some cases, these mechanisms can give rise to large positive (excluded volume) or negative (complexation) cross-diffusion coefficients, sometimes referred to as off-diagonal elements of the diffusivity matrix **D**.

In the Fickian interpretation of the diffusion process, reaction-diffusion equations that include cross-diffusion terms take the following form:

$$\partial u_i/\partial t = R_i(\mathbf{u}) + D_{ii}\nabla^2 u_i + \sum_{j\neq i} \mathrm{div}(D_{ij}\nabla u_j) \qquad (1)$$

$$i, j = 1, 2, .., N$$

where the term $\Sigma\mathrm{div}(D_{ij}\nabla u_j)$ takes into account the flux of species u_i, $D_{ij}\nabla u_j$, induced by the gradient of species u_j. Note that Equation (1) can include unreactive species, for which the reactive term $R_i(\mathbf{u})$ equals zero. Note also that a full treatment of cross-diffusion effects in reaction-diffusion systems requires analysis of the underlying chemical potentials, a procedure more difficult both theoretically and in connecting to experiment than utilizing Equation (1). To analyze the role of the off-diagonal elements, D_{ij}, in pattern formation, we first need to be able to measure them. There are several methods for obtaining cross-diffusion coefficients. The most commonly used are interferometry techniques[2,3] and the Taylor dispersion method.[4–6] Here we employ the latter approach.

We have chosen to study the Belousov–Zhabotinsky (BZ) reaction dispersed in water-in-oil aerosol OT (AOT) microemulsion, (BZ–AOT system),[7–9] where large cross-diffusion effects (for example, a flux of water molecules induced by a flux of AOT molecules) are well documented[10–12] and where a rich array of patterns, including Turing patterns, standing waves, and several types of traveling waves[9,13] have been observed. In recent studies[14,15] we have mea-

[a] Dr. F. Rossi, Dr. V. K. Vanag, Prof. I. R. Epstein
Department of Chemistry and Volen Center for Complex System
MS 015, Brandeis University, Waltham MA 02454-9110 (USA)
E-mail: epstein@brandeis.edu

[b] Dr. F. Rossi
Department of Chemistry, University of Siena and
Polo Universitario Colle Val d'Elsa, Siena (Italy)

[c] Dr. V. K. Vanag
Department of Biology, Lomonosov Moscow State University
Moscow 119899 (Russia)

sured cross-diffusion coefficients in quaternary systems (three solutes + solvent), where the solutes were water (1), AOT (2) and a component of the BZ reaction (3), and the solvent (the continuous phase) was octane. These studies revealed large cross-diffusion coefficients (both positive and negative), D_{13} and D_{23}, that is, large fluxes of water and/or AOT molecules induced by a gradient of a single component of the BZ system.

However, to assess the effects of cross-diffusion on pattern formation in the BZ–AOT system, we require the cross-diffusion coefficients for pairs of species that participate in the BZ reaction. To do this, we must investigate a five-component (pentanary) system, where three components, 1 (water), 2 (AOT), and 5 (octane), are the same as in the earlier quartenary system, while components 3 and 4 are reactive BZ species. In this study, we first introduce our method for finding cross-diffusion coefficients in pentanary systems. We then present our experimental data for two couples: Br^-–Br_2 and ferroin–Br_2. We introduce an alternative procedure for fitting experimental data by using simulations of a set of partial differential equations (PDE) corresponding to the Taylor dispersion method. Finally, we discuss the likely effects of the cross-diffusion coefficients found in this study on pattern formation in BZ–AOT systems.

Results and Discussion

General analysis of a five component BZ–AOT system: In a pentanary systems (four solutes + solvent), the diffusion matrix **D** contains 16 elements, namely 4 diagonal main diffusion coefficients, D_{ii}, and 12 off-diagonal cross-diffusion coefficients D_{ij}, $i, j = 1, 2, 3, 4$ ($i \neq j$).

$$\begin{bmatrix} D_{11} & D_{12} & D_{13} & D_{14} \\ D_{21} & D_{22} & D_{23} & D_{24} \\ D_{31} & D_{32} & D_{33} & D_{34} \\ D_{41} & D_{42} & D_{43} & D_{44} \end{bmatrix} \quad (2)$$

If we consider all 16 elements of **D** as unknowns, then the equations for D_{ij} become so cumbersome that it is extremely difficult to manipulate them to extract the diffusion coefficients. We choose instead to "borrow" 14 elements from experiments on three- and four-component subsystems, assuming that these simpler systems do not change significantly upon addition of a new BZ species. The three-component water-in-oil microemulsion, H_2O/AOT/octane, gives us the coefficients D_{11}, D_{12}, D_{21}, and D_{22}. A four-component subsystem, H_2O/AOT/BZ1/octane, with only one BZ species, BZ1, provides the coefficients D_{13}, D_{23}, D_{31}, D_{32}, and D_{33}. A second four-component subsystem, H_2O/AOT/BZ2/octane, yields D_{14}, D_{24}, D_{41}, D_{42}, and D_{44}. We then need to find only the coefficients D_{34} and D_{43}.

Using the Taylor dispersion technique,[4,5] which involves the diffusive spreading of a drop of solution injected into a laminarly flowing stream containing the same components at slightly different concentrations, we can calculate the so-called dispersion coefficients, F_{ij}, of the matrix **F**, which links the partial derivatives of the concentrations c_i of all components in the flowing stream:[15]

$$\frac{\partial c_i}{\partial t} = \sum_{j=1}^{4} F_{ij} \frac{\partial^2 c_j}{\partial z^2} \quad (3)$$

The dispersion coefficients F_{ij} have the same dimensions as the diffusion coefficients D_{ij} [$cm^2 s^{-1}$], but numerically they are inversely proportional to D_{ij}.[4,5,15] The matrices **F** and **D** are linked by the expressions:

$$D_{ij} = K_{FD} \det(\mathbf{M}_{Fji})(-1)^{(i+j)}/\det(\mathbf{F}) \quad (4)$$

$$F_{ij} = K_{FD} \det(\mathbf{M}_{Dji})(-1)^{(i+j)}/\det(\mathbf{D}) \quad (5)$$

where $K_{FD} = R_0^2 u_0^2/48$ and $\mathbf{M}_{Fji}$ ($\mathbf{M}_{Dji}$) is the minor associated with the corresponding element of matrix **F** (**D**). The coefficients F_{ij} can be obtained from the experimentally found parameters $P_{i,exp}$, K_i, and σ_i through the following equations:[14,15]

$$l_0^{-1} \sum_{i=1}^{n} P_{i,exp} = \sum_{i=1}^{n} K_i c_{i0} \quad (6)$$

$$l_0^{-1} \sum_{i=1}^{n} \sigma_i P_{i,exp} = \sum_{j=1}^{n} c_{i0} \sum_{i=1}^{n} K_i F_{ij} \quad (7)$$

where $n = 4$, l_0 is the length of the section of the capillary occupied by the initially injected sample ($l_0^{-1} = \pi R_0^2/V_0$, V_0 is the injected volume, R_0 is the inner radius of the tube), $P_{i,exp}$ are the pre-exponential parts of the Gaussian functions used to fit the experimental peaks, σ_i are the dispersions of the Gaussian functions, which are equal to the eigenvalues of the dispersion matrix **F**, c_{i0} is the difference between the concentration of component i in the injected sample and in the carrier stream, K_i is the instrumental sensitivity to that component (typically linear in the concentration). The experimentally measurable quantities $P_{i,exp}$, K_i, and σ_i can be found by fitting a set of experimental peaks $v(t)$ generated by injections of different compositions according to

$$v(t) = \sum_{i=1}^{4} \frac{P_{i,exp}}{\sqrt{4\pi\sigma_i t}} \exp\left[-\frac{u_0^2 (t - t_0)^2}{4\sigma_i t}\right] \quad (8)$$

where u_0 is the mean velocity of the carrier stream, and t_0 is the retention time (roughly speaking, t_0 corresponds to the maximum or minimum of the Taylor peak).

In principle, by combining the aforementioned 14 diffusion coefficients with the fitting parameters from a set of experiments, we can find all 16 elements of **F**, and then using

Equations (4) and (5) we can obtain the unknown coefficients D_{34} and D_{43} as well as tune the "known" coefficients D_{ij}.[14] Note that in general we need just two independent Taylor experiments to find the two coefficients D_{34} and D_{43}. However, more experiments with different initial conditions are required to determine the dispersions σ_i with good precision.

As an example, the relatively simple expressions for F_{33} and F_{44} are

$$F_{33} = \frac{\sigma_1\sigma_2\sigma_3\sigma_4}{s_1 s_2 s_4} \tag{9}$$

$$F_{44} = \frac{\sigma_1\sigma_2\sigma_3\sigma_4}{s_1 s_2 s_3} \tag{10}$$

where the s_i are the dispersions of the Gaussian functions obtained by fitting the experimental peaks in the H_2O/AOT/BZ (1 or 2)/octane subsystem. Expressions for the other F_{ij} are much more cumbersome and not of practical use when the dispersions are obtained in experiments with a refractive index detector (RID), because the RID records peaks that are a combination of signals generated by all components, which then requires that Equations (4)–(7) be solved for $n=4$, a step that can introduce significant error in the final results.

If, however, we have a detector that can measure the Taylor peak for a single species in an n-component system, the situation becomes much more favorable. In our system, with Br_2 or ferroin as the BZ component, using a UV-visible spectrophotometer at an appropriate wavelength provides a detector sensitive only to that species, considerably simplifying Equations (6)–(7).

For example, with Br_2 as the only absorbing species in the visible range, the sensitivity coefficients for the other components, K_i^λ ($i=1, 2, 3$) (we rename the coefficients K_i as K_i^λ for UV/Vis measurements at wavelength λ), are zero, and Equations (6) and (7) simplify to:

$$l_0^{-1}\sum_i P_{i,\mathrm{exp\_4}} = K_4^\lambda c_{40} \qquad i = 1-4 \tag{11}$$

$$K_4^\lambda F_{4i} = W_i \qquad i = 1-4 \tag{12}$$

with $W_i = l_0^{-1}(\sum_{j=1}^{4}\sigma_j P_{j,\mathrm{exp\_i}})c_{i0}$, $i, j=1$–4. $P_{j,\mathrm{exp\_i}}$ is the amplitude obtained for the jth Gaussian by fitting the experiment in which only $c_{i0} \neq 0$. The F_{4i} can thus be measured directly from the spectrophotometric curves. The value of F_{44} found from direct measurements via Equation (12) can be compared with the value calculated from Equation (10) to test the method. The value of F_{43} is used to find D_{34} and D_{43}. In fact, we need two equations that relate the desired diffusion coefficients to the known D_{ij} and the experimental data like the dispersions σ_i. One equation is given by the constraint[15]

$$\det(\mathbf{F})\det(\mathbf{D}) = K_{FD}^4 \tag{13}$$

with $\det(\mathbf{F}) = \sigma_1\sigma_2\sigma_3\sigma_4$. For the other, we use Equation (5) for F_{43}:

$$F_{43} = -\frac{\sigma_1\sigma_2\sigma_3\sigma_4}{K_{FD}^3}\det(\mathbf{M}_{D34}) \tag{14}$$

where $\mathbf{M}_{D34} = \begin{bmatrix} D_{11} & D_{12} & D_{13} \\ D_{21} & D_{22} & D_{23} \\ D_{41} & D_{42} & D_{43} \end{bmatrix}$.

So, if we know F_{43}, we can calculate D_{43} from Equation (14) as

$$D_{43} = \frac{\sigma_1\sigma_2\sigma_3\sigma_4(D_{11}D_{23}D_{42} - D_{12}D_{23}D_{41} + D_{13}D_{22}D_{41} - D_{13}D_{21}D_{42}) - F_{43}K_{FD}^3}{\sigma_1\sigma_2\sigma_3\sigma_4(D_{11}D_{22} - D_{12}D_{21})} \tag{15}$$

The coefficient D_{34} can then be obtained from Equation (13), though this expression is rather cumbersome and may lead to relatively large errors in D_{34}. Nevertheless, when F_{34} is known, D_{34} can be found in a manner similar to D_{43}. If F_{34} is unknown, and also as a check on the calculation when F_{34} is known, it is useful to have alternative fitting procedures to obtain D_{34}. If we have several experimental Taylor peaks, we can fit them by a sum of Gaussians via Equation (8), where the dispersions σ_i are calculated from the matrix $\mathbf{F}$ using Equation (5), with D_{34} as the fitting parameter.

Another possible fitting procedure is to integrate the partial differential Equations (3), and compare the results with experiment using both coefficients, D_{34} and D_{43}, as fitting parameters. We discuss this procedure below.

When the two BZ species, as in the case of Br_2 and ferroin, absorb at different wavelengths, we can obtain two Taylor peaks under the same conditions, for example, at $\lambda=400$ and 510 nm. We can then extract the Taylor peaks for the individual species by solving the two simultaneous equations: $A_\lambda/l_c = \varepsilon_{\lambda\_B}[Br_2] + \varepsilon_{\lambda\_f}[\text{ferroin}]$, where A_λ is the absorbance at wavelength λ (=400 nm and 510 nm), ε_{λ_B} and ε_{λ_f} are the molar extinction coefficients for Br_2 and ferroin, respectively, at the two wavelengths, and l_c is the length of the optical path.

The five-component system H_2O (1)/AOT (2)/NaBr (3)/Br_2 (4)/octane (5): When NaBr and Br_2 are the third and fourth components, we can follow the dispersion peaks of bromine at a chosen wavelength in the range $350 \leq \lambda \leq 500$ nm. Figure 1 shows the spectrophotometric peaks at $\lambda=500$ nm, obtained by injecting an excess of bromine ($\Delta[Br_2]=0.1$ M, squares) and an excess of sodium bromide ($\Delta[NaBr]=0.02$ M, triangles) into a flowing solution with $[H_2O]=3.56$ M, $[AOT]=0.3$ M, $[NaBr]=5$ mM and $[Br_2]=0.1$ M. The two dispersion curves were simultaneously fitted to Equation (8) to yield $\sum_i P_{i,\mathrm{exp\_3}} = 1.15$ o.u. × cm and $\sum_i P_{i,\mathrm{exp\_4}} = 11.48$ o.u. × cm, $i=1$, 2, 3, 4. The dispersion σ_4 was found to be 0.4 $cm^2 s^{-1}$, a value close to the dispersion for bromine in the

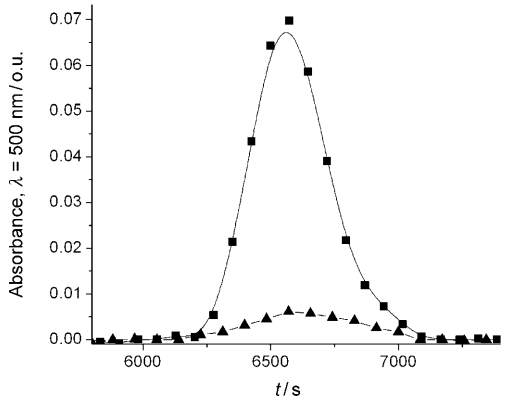

Figure 1. Spectrophotometric signals of Taylor dispersion peaks in the system H_2O/AOT/NaBr/Br_2. ■: $\Delta[Br_2]=0.1$ M; ▲: $\Delta[NaBr]=0.02$ M. Composition of the flowing solution: $[H_2O]=3.56$ M, $[AOT]=0.3$ M, $[NaBr]=5$ mM and $[Br_2]=0.1$ M. $T=23$ °C. $\lambda=500$ nm. Solid lines represent analytical signals built by using the diffusion coefficient matrix in Table 1.

subsystem H_2O/AOT/Br_2. More precise values for the other dispersions were found by fitting the RID peaks shown in Figure 2 to give $\sigma_1=6.84\,cm^2s^{-1}$, $\sigma_2=7.14\,cm^2s^{-1}$ and $\sigma_3=16.71\,cm^2s^{-1}$. From Equation (11) we calculated $K_4^{500}=32$ o.u./M, which agrees with the product $l_c \times \varepsilon_{500}$ for bromine ($l_c=1$ cm). The peak generated by injecting an excess of NaBr reveals the presence of a flow of bromine coupled to the diffusion of sodium bromide and allows us to calculate F_{43} from Equation (12) and in turn D_{43} from Equation (15). The coefficients F_{41} and F_{42} were found to be close to zero, that is, no peaks were detected, which implies that the flux of bromine induced by water or by the surfactant is very low, as was the case in the quaternary subsystem. In order to check the results, F_{44} was determined from our experimental measurements using Equation (12). The value obtained, $0.32\,cm^2s^{-1}$, was in excellent agreement with the theoretical value of $0.30\,cm^2s^{-1}$ obtained from Equation (10).

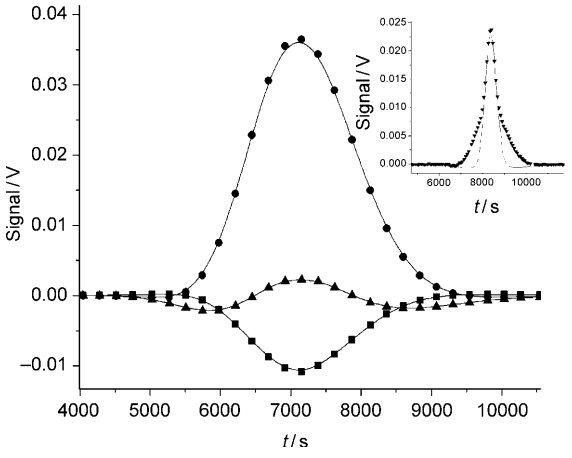

Figure 2. RID signals of Taylor dispersion peaks in the system H_2O/AOT/NaBr/Br_2. ■: $\Delta[H_2O]=1.5$ M; ●: $\Delta[AOT]=0.2$ M; ▲: $\Delta[NaBr]=0.02$ M. Solid lines represent analytical signals built by using the diffusion coefficient matrix in Table 1. Inset shows the RID peak when an excess of bromine ($\Delta[Br_2]=0.1$ M) is injected in the flowing solution.

The diffusion coefficient matrix for the system H_2O (1)/AOT (2)/NaBr (3)/Br_2 (4)/octane is reported in Table 1. The value of D_{34} was found by fitting the analytical signals to the RID peaks reported in Figure 2, while the diffusivities for the two quaternary subsystems were taken from ref. [14]. The inset of Figure 2 shows that, in contrast with the other samples, the peak generated when an excess of Br_2 is injected does not give good agreement between the calculated signal and the experimental data. We tentatively attribute this discrepancy to a non-negligible concentration of tribromide ion, Br_3^-, resulting from the relatively high concentration of bromine required to get a good signal-to-noise ratio.

Table 1. Pentanary diffusion coefficients (in $10^{-6}\,cm^2s^{-1}$) for H_2O (1)/AOT (2)/NaBr (3)/Br_2 (4) system at $\omega=11.84$, $\phi_d=0.18$, $[NaBr]=5$ mM and $[Br_2]=10$ mM, and $T=23$ °C.

j	D_{j1}	D_{j2}	D_{j3}	D_{j4}
1	0.63 ± 0.04	6.60 ± 3	80.9 ± 10	-130 ± 20
2	-0.01 ± 0.2	1.21 ± 0.2	4.75 ± 0.8	-2.7 ± 0.09
3	0.002 ± 0.003	-0.04 ± 0.02	0.47 ± 0.1	-0.83 ± 0.2
4	0.06 ± 0.15	-0.98 ± 0.3	-0.13 ± 0.03	19.2 ± 3

The five component system H_2O (1)/AOT (2)/ferroin (3)/Br_2 (4)/octane (5): The pentanary diffusion coefficient matrix obtained when ferroin and Br_2 are the two BZ components is reported in Table 2 for a microemulsion system with $\omega=11.84$ and $\phi_d=0.10$. The diffusivities for the ferroin quaternary sub-system were taken from ref. [14], while those for the bromine sub-system (D_{14}, D_{24}, D_{41}, D_{42}, D_{44}) have been determined in the present work. As in the case of ferroin,[14] they were found to depend upon the microemulsion composition (ω and ϕ_d).

Table 2. Pentanary diffusion coefficients (in $10^{-6}\,cm^2s^{-1}$) for the H_2O (1)/AOT (2)/ferroin (3)/Br_2 (4) system at $\omega=11.84$, $\phi_d=0.1$, [ferroin] = 0.1 mM, $[Br_2]=5$ mM, and $T=23$ °C.

j	D_{j1}	D_{j2}	D_{j3}	D_{j4}
1	1.28 ± 0.07	1.76 ± 0.7	-137 ± 22	-298 ± 48
2	-0.005 ± 0.0008	1.51 ± 0.3	-28 ± 0.9	-18.8 ± 0.6
3	-0.00038 ± 0.0009	0.0025 ± 0.0006	0.96 ± 0.1	-0.02 ± 0.003
4	0.0005 ± 0.001	-0.07 ± 0.02	-15.6 ± 3	30 ± 4

In this case, we utilized a different procedure to find the two unknown cross-diffusion coefficients, D_{34} and D_{43}, because we were able to take advantage of the fact that both species absorb in the visible range. The ferroin absorption maximum occurs at $\lambda=510$ nm (ε_{510} ~13800 $M^{-1}cm^{-1}$). Therefore, when an excess of either bromine or ferroin is injected into the flowing solution, the flux induced in the other BZ component can be recorded at the wavelength of its absorption maximum. Following this procedure, we monitored the absorption of ferroin when an excess of bromine was injected. No peaks could be detected at $\lambda=510$ nm,

which implies that under our experimental conditions D_{34} is quite small.

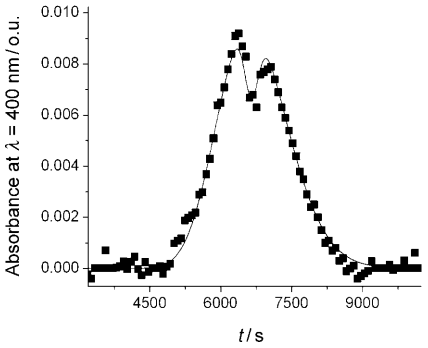

Figure 3. System H_2O/AOT/ferroin/Br_2. Squares show spectrophotometric peak recorded at $\lambda = 400$ nm (bromine maximum absorbance wavelength) when an excess of ferroin was injected (Δ[ferroin] = 1 mM). Composition of the flowing solution: [H_2O] = 1.98 M, [AOT] = 0.167 M, [ferroin] = 0.01 mM and [Br_2] = 5 mM. $T = 23$ °C. Solid lines represent analytical signals built by using the diffusion coefficient matrix in Table 2.

In contrast, Figure 3 presents the dispersion curve recorded at $\lambda = 400$ nm generated by injection of a sample containing an excess of ferroin. The complex shape of the peak indicates a strongly coupled flow of bromine induced by the gradient of ferroin. In this case, the ferroin has an absorption tail at 400 nm and $K_3^{400} \neq 0$. Equation (7) thus yields

$$F_{43} = \frac{W_3 - K_3^{400} F_{33}}{K_4^{400}} \tag{16}$$

where $F_{33} = 8.24\ \mathrm{cm^2 s^{-1}}$ has been calculated via Equation (12) from an experiment in which the absorbance of a sample containing an excess of ferroin was recorded at $\lambda =$ 510 nm. The coefficients $K_3^{400} = 2065$ o.u./M and $K_4^{400} =$ 175 o.u./M were calculated from Equation (11). Equation (15) finally yields $D_{43} = -1.7 \times 10^{-5}\ \mathrm{cm^2 s^{-1}}$, which accounts for the flux of bromine generated by the gradient of ferroin. The experimental peaks recorded with the RID were used to generate more precise values for the dispersions ($\sigma_1 = 5.5\ \mathrm{cm^2 s^{-1}}$, $\sigma_2 = 5.24\ \mathrm{cm^2 s^{-1}}$, $\sigma_3 = 8.23\ \mathrm{cm^2 s^{-1}}$ and $\sigma_4 = 0.31\ \mathrm{cm^2 s^{-1}}$) and to test and refine the diffusion matrix **D**.

Figure 4 shows the analytical signals built by using the diffusion matrix of Table 2 for a sample containing an excess of bromine, a) Δ[Br_2] = 0.1 M, and a sample containing an excess of ferroin, b) Δ[Fe] = 1 mM. The fitting and refinement procedure also allowed us to calculate $D_{34} = -2 \times 10^{-8}\ \mathrm{cm^2 s^{-1}}$, which was not directly measurable in our spectrophotometric experiments. Finally, values for F_{33} and F_{44} (8.64 and 0.34 $\mathrm{cm^2 s^{-1}}$, respectively) were calculated from Equation (10) and compared with those from our UV/Vis experiments (8.24 and 0.31 $\mathrm{cm^2 s^{-1}}$, respectively). Again, the agreement is quite good.

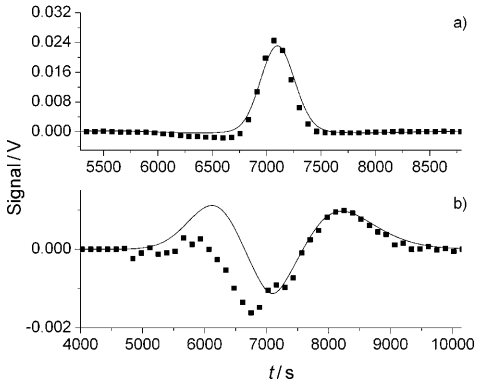

Figure 4. System H_2O/AOT/ferroin/Br_2. a) RID peak recorded when an excess of bromine was injected (Δ[Br_2] = 0.1 M). b) RID peak recorded when an excess of ferroin was injected (Δ[Fe] = 1 mM). Composition of the flowing solution: [H_2O] = 1.98 M, [AOT] = 0.167 M, [ferroin] = 0.01 mM and [Br_2] = 5 mM. $T = 23$ °C. Solid lines represent analytical signals built by using the diffusion coefficient matrix in Table 2.

PDE fitting: A key step in the Taylor dispersion method for determining cross-diffusion coefficients is the fitting of the experimental signal by a set of Gaussians to find the parameters $P_{i,exp}$, K_i, and σ_i. If there are N components (5 in our case), then the number of Gaussian functions is $N-1$ for each experimental run. In principle, different runs with different injected solutions should give identical sets of σ_i. In practice, as N increases, and one attempts to fit multiple experiments, one is increasingly likely to encounter shallow local minima in attempting to optimize σ_i by minimizing the difference between the experimental and fitted curves. Therefore, for large N it is desirable, as a check on the direct fitting method, to have an independent procedure to generate the elements of **D**, thereby allowing us to choose between alternative sets of σ_i that give comparable agreement between calculation and experiment. Here we describe an approach in which the F_{ij} [or the D_{ij} via Eqs. (4) and (5)] are obtained by numerically integrating Equations (3) and optimizing the agreement between the calculated and experimental concentration profiles.

As before, we take all the D_{ij} except D_{34} and D_{43} from experiments on the ternary and quaternary subsystems and seek to determine the latter two coefficients from experiments on the pentanary system. We use the coefficients in Table 1 for the Br^-–Br_2 system and those in Table 2 for the ferroin–Br_2 system. To calculate the F_{ij} we use Equation (5), which transforms the coefficients D_{ij} to F_{ij}. For a given set of D_{ij} we integrate the partial differential Equations (3) in one spatial dimension (x) using the commercially available software package FlexPDE,[16] with a typical error (ERRLIM) of 1.0×10^{-7} for each variable in each spatial cell. We then vary D_{34} and D_{43} in an attempt to improve the agreement. Although it is possible to do a rigorous minimization of, for example, the sum of squares of pointwise differences between the calculated and experimental curves, here, for reasons discussed below, we seek only a qualitative agreement, which is sufficient to select between alternative sets of σ_i.

Since Equations (3) are linear, only deviations from the initial concentrations c_{i0} are important. Therefore we normalize the variables by setting $c_{i0}=1$ as the set of "concentrations in the flowing stream". Initial perturbation of one of the four variables, which is equivalent to injection of a sample in the Taylor experiment, is made in a narrow (1 cm) region l_0 at the center of a long ($\geq$ 10 m) one-dimensional segment that represents our coiled capillary. Again, since Equations (3) are linear, the amplitude of the perturbation does not affect the shape of the resulting curves (in our computer simulation, unlike the actual Taylor experiment, we do not have problems with the sensitivity of the detector). We typically take the amplitude of this perturbation as $0.1c_{i0}$. Since the amplitude and dispersion (σt) of the Gaussian curves (8), where the term $u_0^2(t-t_0)^2$ is replaced by $(x-x_0)^2$, decrease and broaden, respectively, as $(t)^{-1/2}$ and (t), the shape of the curves $c_i(t)$ is almost constant after some initial interval, and the ratio between different maxima and minima remains constant with time. Therefore, for qualitative comparison with the experimental peaks, it is not necessary to simulate Equations (3) for times as long as in the actual experiment. Usually, 100 s is sufficient to yield curves with shapes similar to those at much longer times.

For this set of computer experiments, we use the diffusion coefficients reported in Table 2 except for D_{34} and D_{43}, which are different for different curves and are listed in Table 3. In curves 1–4 (Figure 5a), we study the effect of D_{43} on the Taylor peak measured at 400 nm when c_3 is initially perturbed. We see that the minimum in curves 1–4 becomes deeper as D_{43} is made more negative (max/min = 1.01, 1.18, 1.29, and 1.43 for curves 1–4, respectively, while the experimental ratio from Figure 3 gives max/min $\cong$ 1.26). The range of D_{43} between -1.5×10^{-5} and -2×10^{-5} cm^{2}s^{-1} seems to be appropriate. Note that this result is almost independent of D_{34}, if D_{34} is not too negative. To estimate the value of D_{34}, we build in Figure 5b the curves corresponding to the Taylor dispersion curves recorded by RID (shown in Figure 4). Note that curves 1–5 (when variable c_4 is perturbed) obtained at different D_{34} are almost indistinguishable from one another and correspond well to the experimental curve in Figure 4b. The same is true of curves 1′–5′ (when c_3 is perturbed) of Figure 5b and the experimental curve in Figure 4a. However, if D_{34} is too negative (e.g., -2×10^{-7} cm^{2}s^{-1}), then large positive wings, which are not observed in the experiment, emerge (see curve 6″ in Figure 5b). These simulations clearly show the lower negative limit for D_{34}, but an accurate (even to 50%) value of D_{34} is difficult to determine by this method.

With $D_{34}=-2\times10^{-8}$ cm^{2}s^{-1} and the other diffusion coefficients assigned the values in Table 2, choosing D_{43} between -1.5×10^{-5} and -2×10^{-5} cm^{2}s^{-1} enables us to match the ratio between the minimum and the two maxima in the experimental absorbance, Figure 3, while also reproducing the RID curves in Figure 4. The coefficient D_{43} alone determines the shape of the curve in Figure 3 (when an excess of ferroin is injected). Indeed the other two cross-diffusion coefficients, D_{41} and D_{42}, are too small to account for the flux of Br_2 generated by the gradient of ferroin. The ferroin gradient induces fluxes of H_2O and AOT that in turn can generate a flux of Br_2. This fitting procedure thus provides a route to determining cross-diffusion coefficients to an accuracy better than 50%. Reassuringly, the cross-diffusion coefficient D_{43} obtained by the PDE fitting is in good agreement with the value obtained from the usual fitting procedure in which Gaussian curves [Eq. (8)] are used and where the error in D_{34} and D_{43} is between 15 and 20%. We will see in the next section that the accuracy provided by the PDE fitting technique is more than sufficient for assessing the role of cross-diffusion in pattern formation in the BZ–AOT system.

Table 3. Values of D_{34} and D_{43} used to build curves in Figure 5. Diffusion coefficients are in units of cm^{2}s^{-1}.

Curve	1	2	3	4	5	6
D_{34}	-2×10^{-8}	-2×10^{-8}	-2×10^{-8}	-2×10^{-8}	-2×10^{-9}	-2×10^{-7}
D_{43}	-0.5×10^{-5}	-1.5×10^{-5}	-2×10^{-5}	-2.5×10^{-5}	-2×10^{-5}	-2×10^{-5}

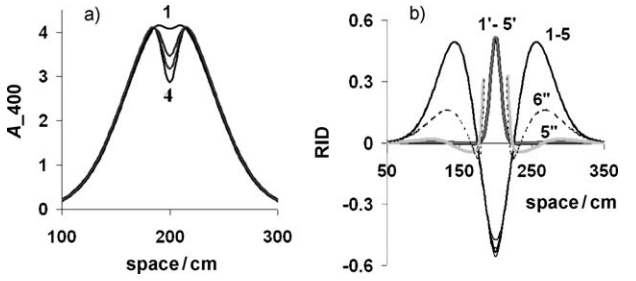

Figure 5. Solutions of Equations (3) at $t=100$ s with different sets of F_{ij} presented as a) "A_400" (absorption at 400 nm) and b) "RID" for the ferroin (c_3)/Br_2 (c_4) system. "A_400" $=l(c_3\varepsilon_{400\_f}+c_4\varepsilon_{400\_B})$ with $\varepsilon_{400\_f}=2075\,\mathrm{M}^{-1}\mathrm{cm}^{-1}$, $\varepsilon_{400\_B}=175\,\mathrm{M}^{-1}\mathrm{cm}^{-1}$, and $l=1$ cm; RID $=K_1c_1+K_2c_2+K_3c_3+K_4c_4$ with $K_1=-2.8$, $K_2=44$, $K_3=180$, and $K_4=11\,\mathrm{V\,M}^{-1}$ To obtain the matrix **F**, we use the diffusion coefficients reported in Table 2, except for D_{34} and D_{43} for which we used the values reported in Table 3. For curves marked by prime and double prime, c_4 (Br_2) is initially perturbed, while for all other cases, c_3 (ferroin) is perturbed. Curves 5″ and 6″ show 50 × RID, while curves 1′–5′ in **b** show 4× RID; curves 5 and 3 coincide in **a**.

Effects of cross-diffusion in a BZ–AOT model: We consider now the possible effects of cross-diffusion coefficients of the magnitude found experimentally on pattern formation in the BZ–AOT system. This system demonstrates a wide variety of patterns that arise via several different pattern-formation mechanisms.[9,17,18] We do not attempt to examine the role of cross-diffusion in all of them here, but rather restrict ourselves to an analysis of Turing patterns.[13,19] We choose Turing patterns in large measure because this behavior does not arise in the aqueous BZ system, whereas it is a prominent feature of the BZ–AOT system. Earlier analyses[13] have suggested that BZ–AOT Turing patterns arise because the inhibitor species Br_2 diffuses more rapidly through the oil

than the activator, which is confined to the aqueous droplets and diffuses at the much slower rate of whole droplets. A four-variable model of the BZ–AOT system[20] that we recently proposed includes the species $x=[HBrO_2]$, $y=[Br^-]$, $z=$[ferriin] and $u=[Br_2]$:

$$\mathrm{d}x/\mathrm{d}t = -k_1xy + k_2y - 2k_3x^2 + k_4x(c_0-z)/(c_0-z + c_{min}) + \mathrm{div}[D_{XX}\mathrm{grad}(x)] \quad (17)$$

$$\mathrm{d}y/\mathrm{d}t = -3k_1xy - 2k_2y - k_3x^2 + k_7u + k_9z + \mathrm{div}[D_{YY}\mathrm{grad}(y) + D_{YU}\mathrm{grad}(u)] \quad (18)$$

$$\mathrm{d}z/\mathrm{d}t = 2k_4x(c_0-z)/(c_0-z + c_{min}) - k_9z - k_{10}z + \mathrm{div}[D_{ZZ}\mathrm{grad}(z) + D_{ZU}\mathrm{grad}(u)] \quad (19)$$

$$\mathrm{d}u/\mathrm{d}t = 2k_1xy + k_2y + k_3x^2 - k_7u + \mathrm{div}[D_{UU}\mathrm{grad}(u) + D_{UY}\mathrm{grad}(y) + D_{UZ}\mathrm{grad}(z)] \quad (20)$$

where c_0 is the total concentration of the catalyst and ${c_{min}}^2 = 2k_r(k_9 + k_{10})c_0/{k_{red}}^2$. The (nearly constant) concentrations $[H^+]$, $[BrO_3^-]$, and malonic acid [MA] are incorporated into the constants given in the caption to Figure 6, grad $=\partial/\partial r$, where r is the spatial coordinate in one dimension.

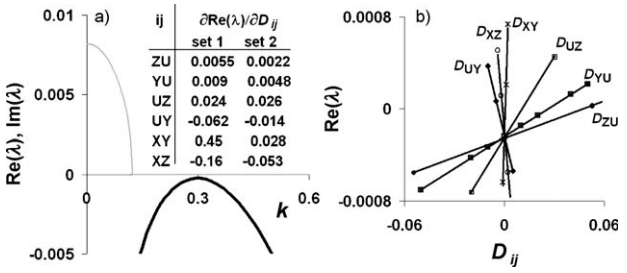

Figure 6. a) Dispersion curve for Equations (17)–(20) at the onset of Turing instability. Bold line is Re(λ) and thin gray line is Im(λ) for the largest eigenvalue λ. b) Dependence of the maximum of Re(λ) on the cross-diffusion coefficient D_{ij} with all other $D_{ij}=0$ ($i \neq j$). Parameter set 1: $k_1=56000\,M^{-1}s^{-1}$, $k_2=0.000314\,s^{-1}$, $k_4=0.2352\,s^{-1}$, $k_7=0.163125\,s^{-1}$, $k_9=0.0405\,s^{-1}$, $k_{10}=0.0225\,s^{-1}$, which corresponds to concentrations $[H^+]=0.028\,M$, $[BrO_3^-]=0.2\,M$, and $[MA]=0.45\,M$; $c_0=0.003\,M$, $k_3=2000\,M^{-1}s^{-1}$, $k_r=10^7\,M^{-1}s^{-1}$, $k_{red}=2\times10^6\,M^{-1}s^{-1}$, $D_{XX}=D_{YY}=0.06$, $D_{ZZ}=0.05$. All diffusion coefficients are normalized so that $D_{UU}=1$. Inset to panel a) shows sensitivities $\partial\mathrm{Re}(\lambda)/\partial D_{ij}$ (with all other $D_{ij}=0$) for parameter sets 1 and 2. Set 2 has almost the same dispersion curve as shown in panel a) with the Re(λ)-k curve nearly tangent to the abscissa. For set 2, $k_1=7800\,M^{-1}s^{-1}$, $k_2=6.08\times10^{-6}\,s^{-1}$, $k_4=0.03276\,s^{-1}$, $k_7=0.145\,s^{-1}$, $k_9=0.016\,s^{-1}$, $k_{10}=0.02\,s^{-1}$, which corresponds to $[H^+]=0.0039\,M$, $[BrO_3^-]=0.2\,M$, and $[MA]=0.4\,M$; $D_{XX}=D_{YY}=0.1$, c_0, k_3, k_r, k_{red}, and D_{ZZ} as in set 1.

Using this model, we can investigate how the cross-diffusion coefficients D_{YU}, D_{ZU}, D_{UY}, and D_{UZ} can affect the onset of Turing instability. The simplest way to do this is to perform a linear stability analysis of Equations (17)–(20). Note that the cross-diffusion coefficients must depend upon the corresponding concentrations as $D_{YU}(y)$, $D_{ZU}(z)$, $D_{UY}(u)$, and $D_{UZ}(u)$, tending to zero as the corresponding concentration tends to zero. However, we do not know these dependences at present, so we treat these coefficients as constants. We should bear in mind, however, that the true absolute values of these coefficients at the steady state concentrations of the variables of Equations (17)–(20) may be smaller than those we have found, because our experiments are conducted at higher concentrations than the steady state values and we expect the dependence of the cross-diffusion coefficients on concentration to be monotonic.

In Figure 6a, we show a dispersion curve obtained from linear stability analysis of our model with all $D_{ij}=0$ ($i \neq j$) at a set of parameters ($[H^+]$, $[BrO_3^-]$, and [MA]) for which the system is very close to the onset of Turing instability. We then vary the cross-diffusion coefficients to see how the maximum of the curve Re(λ) responds to these changes. The results of these calculations are shown in Figure 6b and in the inset to Figure 6a, which contains the sensitivities, $\partial\mathrm{Re}(\lambda)/\partial D_{ij}$ (where indices i and j here correspond to variables x, y, z, and u) for two sets of parameters. We see, for example, that a negative value of D_{UY} ($=D_{43}/D_{44}=-0.13/19.2 \cong -0.007$, from Table 1) can switch a negative maximum of Re(λ) to a positive one, that is, can result in Turing patterns, if this maximum is initially close to zero. Approximately the same increase in max[Re(λ)] occurs if we increase, for example, $[BrO_3^-]$ by 5–10% or decrease [MA] by 5–10%. In contrast to D_{UY}, a negative D_{YU} decreases max[Re(λ)]. However, the sensitivity of max[Re(λ)] to D_{YU} is 3–7 times smaller than that to D_{UY}. This sensitivity of max[Re(λ)] to D_{ij} can be estimated from the values of $\partial\mathrm{Re}(\lambda)/\partial D_{ij}$ (see Figure 6a).

Analyzing the sensitivity of max[Re(λ)] on other cross-diffusion coefficients, we find that the most sensitive parameter is D_{XY}, and then D_{XZ}. Unfortunately, we are unable to measure these cross-diffusion coefficients directly because of the chemical instability of species X ($HBrO_2$).

Conclusion

To the best of our knowledge, the experiments reported here constitute the first measurements of cross-diffusion coefficients in a five-component system. The modified Taylor dispersion method,[15] developed initially for a three-component system, has been applied to a four-component system[14] and now to a five-component system. To alleviate potential numerical difficulties associated with the larger system, we have introduced an alternative fitting procedure involving the solution of a set of PDE [Eq. (3) with matrix **F**] with variable diffusion coefficients D_{ij} linked to the coefficients F_{ij} via Equations (4) and (5).

The cross-diffusion coefficients that characterize the interaction between two key species of the BZ system, namely D_{34} and D_{43}, were found to be negative for both systems analyzed. The negative sign of these coefficients signifies that species 3 is attracted toward higher concentrations of species 4 and vice versa, and, for both Br^- and ferroin, complexation with Br_2 lies at the origin of the cross-diffusion mecha-

nism. This complexation process probably also accounts for the relatively poor agreement between the analytical and experimental peaks in the inset of Figure 2 and in panel b) of Figure 4.

The values we have found for the cross-diffusion coefficients are sufficient to generate a shift in the onset of Turing instability comparable to the effect produced by increasing $[BrO_3^-]$ or decreasing [MA] by 5–10%. The dependence of the cross-diffusion coefficients on the species concentrations makes the diffusive terms $\mathrm{div}[D_{ij}\mathrm{grad}(u_j)]$ nonlinear and may lead not only to a shift in the onset of bifurcation, but also to the emergence and stabilization of new forms of dissipative patterns. This strongly nonlinear effect cannot be understood using linear stability analysis alone and may also be challenging for weakly nonlinear analysis, for example, amplitude equations. Direct integration of reaction-diffusion equations is probably required to investigate such possible effects. Another limitation to a full analysis of the possible role of cross-diffusion in pattern formation is a lack of experimental data on cross-diffusion coefficients between pairs of reactive species like activator and inhibitor. We plan to address these problems in future work.

Experimental Section

Experiments were performed using a standard HPLC apparatus with a long capillary (~30 m length, 0.042 cm diameter) in place of the chromatographic column. The flow was kept at a constant velocity of 0.15 mL min^{-1} with an isocratic pump (Agilent G1310 A). The detectors (RID, Agilent 1100 series and UV/Vis spectrophotometer, Shimadzu UV-1650PC) were placed at the end of the capillary. Known volumes (20 μL) of the samples were injected through a Reodine injection system. The capillary and the injection system were kept at constant temperature (23 °C) in a thermostatted incubator (Fisher Scientific).

Sodium bromide (Fisher), bromine (Sigma), ferroin (Fluka) and sodium bis(2-ethylhexyl)sulfosuccinate, AOT (Aldrich) were of analytical grade and used as received. Octane (Sigma) was further purified by mixing with concentrated sulfuric acid for two days. Microemulsion and stock solutions were prepared with doubly distilled water. Further details about the experimental setup and microemulsion preparation can be found elsewhere.[14,15]

Acknowledgements

This work was supported in part by the National Science Foundation through grant CHE-0526866. F.R. was supported by a Marie Curie International Outgoing Fellowship within the 7th European Community Framework Programme. I.R.E. thanks the Radcliffe Institute for a fellowship.

[1] V. K. Vanag, I. R. Epstein, *Phys. Chem. Chem. Phys.* **2009**, *11*, 897–912.
[2] E. L. Cussler, P. J. Dunlop, *J. Phys. Chem.* **1966**, *70*, 1880–1888.
[3] O. Annunziata, A. Vergara, L. Paduano, R. Sartorio, D. G. Miller, J. G. Albright, *J. Phys. Chem. B* **2009**, *113*, 13446–13453.
[4] G. I. Taylor, *Proc. R. Soc. London, Ser. A* **1953**, *219*, 186–203.
[5] W. E. Price, *J. Chem. Soc. Faraday Trans. 1* **1988**, *84*, 2431–2439.
[6] A. Alizadeh, C. A. Nieto de Castro, W. A. Wakeham, *Int. J. Thermophys.* **1980**, *1*, 243–284.
[7] I. R. Epstein, V. K. Vanag, *Chaos* **2005**, *15*, 047510.
[8] V. K. Vanag, *Phys.-Usp.* **2004**, *47*, 923–941.
[9] V. K. Vanag, I. R. Epstein in *Self-Organized Morphology in Nanostructured Materials* (Eds.: K. Al-Shamery, J. Parisi), Springer, Berlin **2008**, p. pp. 89–113.
[10] D. G. Leaist, L. Hao, *J. Phys. Chem.* **1995**, *99*, 12896–12901.
[11] L. Costantino, C. Dellavolpe, O. Ortona, V. Vitagliano, *J. Chem. Soc. Faraday Trans.* **1992**, *88*, 61–63.
[12] L. Costantino, C. Dellavolpe, O. Ortona, V. Vitagliano, *J. Colloid Interface Sci.* **1992**, *148*, 72–79.
[13] V. K. Vanag, I. R. Epstein, *Phys. Rev. Lett.* **2001**, *87*, 228301.
[14] F. Rossi, V. K. Vanag, E. Tiezzi, I. R. Epstein, *J. Phys. Chem. B* **2010**, *114*, 8140–8146.
[15] V. K. Vanag, F. Rossi, A. A. Cherkashin, I. R. Epstein, *J. Phys. Chem. B* **2008**, *112*, 9058–9070.
[16] FlexPDE, http://www.pdesolutions.com **2010**.
[17] V. K. Vanag, I. R. Epstein, *Chaos* **2008**, *18*, 026107.
[18] V. K. Vanag, I. R. Epstein, *Int. J. Dev. Biol.* **2009**, *53*, 673–681.
[19] A. M. Turing, *Philos. Trans. R. Soc. London Ser. B* **1952**, *237*, 37–72.
[20] V. K. Vanag, I. R. Epstein, *J. Chem. Phys.* **2009**, *131*, 104512.

Received: July 20, 2010
Published online: January 19, 2011

